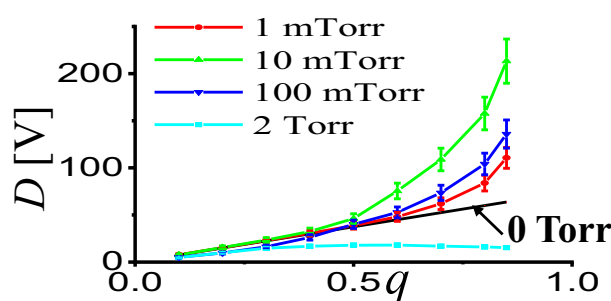


Ion-Neutral Collision Effects on Ion Trapping and Pseudopotential Depth in Ion Trap Mass Spectrometry

Ming Li,^{1,2} Xinwei Liu,² Xiaoyu Zhou,²  Zheng Ouyang²

¹NCS Testing Technology CO., Ltd, Beijing, 100081, China

²State Key Laboratory of Precision Measurement Technology and Instruments, Department of Precision Instrument, Tsinghua University, Beijing, 100084, China



Abstract. Ion trapping using radio-frequency (RF) devices has been widely used in mass spectrometry (MS). The pseudopotential well (PW) model enables the use of a pseudopotential depth, D , to evaluate the ion trapping capability of the RF devices in the pure electric field. It remains unclear how gas pressures regulate the ion trapping and D . Here, we calculated the D of a linear ion trap (LIT) from 1 mTorr to 2 Torr, a pressure range critical for the operation of the RF devices,

through ion cloud simulations. Compared with the case of pure electric field, ion-neutral collision effects at pressures of 1 to 100 mTorr were beneficial for the ion trapping and revealed an optimal trapping depth, D , at around 10 mTorr. We explained the mechanism and validated the observation via ion trapping experiments performed in a home-made dual LIT mass spectrometer. We also showed that near the stability boundary, the RF heating became comparable with the D , which led to the decrement of ion trapping capability characterized by the available D .

Keywords: RF devices, ion trap, ion-neutral collisions, Pseudopotential depth

Received: 25 July 2019/Revised: 7 September 2019/Accepted: 25 September 2019/Published Online: 28 October 2019

Introduction

Radio-frequency (RF) devices originated from the quadrupole ion trap are developed by Paul and Steinwedel in the 1950s [1]. They have been widely employed for ion trapping in mass spectrometry (MS) [2, 3], including ion trap [4–6], mass filter [4–6], ion guide [4–6], ion funnel [7], and ion mobility analyzer [8]. In the RF devices, the RF field varies with time periodically; the ions can be stably trapped within one half of the RF cycle and become unstable in the other half. To trap the ions in the entire RF cycle, the RF phases should change timely before the ions escape from the

devices. Therefore, compared with that using direct current (DC), ion motion in the RF field is more complex. It includes a series of micro-harmonics which do not exist in the DC trapping, other than the secular (or macro-) harmonic. How to evaluate the ion trapping capability of the RF devices, in analogy to the DC counterpart, is a fundamental but very practical question.

The pseudopotential well (PW) model [9–11], which is equivalent to the RF potential by an effective DC, can provide a pseudopotential depth, D , to allow the evaluation of ion trapping capability for the RF devices. It is generally recognized that deeper trapping depths, D , should be beneficial for ion trapping. Using the model, the D has a physical meaning of the energy that an ion must acquire to leave the trapping volume [12, 13]. For linear ion traps (LITs) and linear quadrupoles, they have $D = qV_{RF}/4$, where q is the Mathieu parameter and V_{RF} is the RF voltage applied to the electrodes. The model was originally considered valid only for $q < 0.4$; recent theoretical calculations showed that it

Electronic supplementary material The online version of this article (<https://doi.org/10.1007/s13361-019-02344-x>) contains supplementary material, which is available to authorized users.

Correspondence to: Xiaoyu Zhou; e-mail: zhoyuzxy@mail.tsinghua.edu.cn, Zheng Ouyang; e-mail: ouyang@mail.tsinghua.edu.cn

was valid through the entire first stability region, i.e., q up to 0.908 [12–14]; however, for $q > 0.6$, the model fails to meet the experimental observation of decreased ion trapping efficiencies [15, 16].

Furthermore, due to the development of ambient sampling technologies [17, 18], the RF devices are increasingly applied at elevated pressure ranges [19, 20]. Currently, in most of the laboratory MS instruments with an atmospheric pressure interface (API) [21, 22], ions are generated in atmosphere (760 Torr), transferred by RF ion optics through a differential pressure system (from 2 Torr to 1 mTorr), and mass analyzed at 1×10^{-5} Torr. Mass analysis in miniature mass spectrometers can even be performed at pressures above 1 Torr [23, 24]. The classic PW model, based on ion motion in the pure electric field, can hardly be applied for these scenarios, where the ion motion is increasingly regulated by the gas hydrodynamic field, rather than the electric field [25]. This calls for new physics implemented to allow the modeling and understanding of the classic ion trapping problem.

Here, taking advantage of ion cloud simulations, we numerically measured the pseudopotential depths, D , of a LIT through the extraction of flow properties from an ion cloud at thermal equilibrium. The D values in a pressure range from 1 mTorr to 2 Torr were explored. The RF heating of the ions was also evaluated and used to explain the differences between the numerically calculated trapping depth and experimentally measured ion trapping efficiency.

Method

The LIT used in this study had two, x and y , electrode pairs with a field radius $r_0 = 4$ mm, and the electrode pairs were applied with a quadrupole RF, $V_{RF} = 300$ V_{0-p}, at a frequency $\Omega = 1$ MHz (Figure 1a). The LIT can generate an electric trapping potential ϕ for ion trapping [4], which yields

$$\phi = \left(\frac{x^2 - y^2}{r_0^2} \right) (U - V_{RF} \cos \Omega t) \quad (1)$$

where U is the DC trapping potential applied to the electrodes. The ion motion in the pure electric field is described by the Mathieu equation, characterized by the Mathieu parameters, a_u and q_u , which yield

$$a_x = -a_y = \frac{8ZeU}{m\Omega^2 r_0^2}; \quad q_x = -q_y = \frac{4ZeV_{RF}}{m\Omega^2 r_0^2} \quad (2)$$

where m is ion mass and e and Z are electron charge and charge number of trapped ions, respectively. In the PW model, the RF field can be equivalent to a DC, ϕ_{eff} , with a pseudopotential depth, D [26], which yields

$$\phi_{eff} = \frac{x^2}{r_0^2} (U + D) + \frac{y^2}{r_0^2} (-U + D) \quad (3)$$

The ϕ_{eff} should have the same ion trapping capability as ϕ . In the LIT, due to the presence of background pressures, the ion motion in the electric field is subjected to the stochastic ion-neutral collisions, and the ion distribution, number density n , within the trap follows the convection diffusion equation, which yields

$$J_u = nKE_u - D_{diff} \nabla_u n \quad (u = x \text{ or } y) \quad (4)$$

where u denotes x or y coordinate, J_u is the ion flux, and E_u is the electric field strength. K and D_{diff} represent ion mobility and ion diffusion coefficients, respectively, and they have $K = eD_{diff}/k_b T_{ion}$ according to the Nernst-Townsend-Einstein relation, where k_b is the Boltzmann constant and T_{ion} is the ion temperature in the LIT. At equilibrium, the ion cloud has $J = 0$; the Eq. (4) becomes

$$\nabla_u n = -\frac{eE_u}{k_b T_{ion}} n \quad (5)$$

For $U = 0$, the ion distribution n in the pseudopotential well, $E_u = -\nabla_u \phi_{eff} = 2D \frac{u}{r_0^2}$, has

$$n = n_0 \exp \left[-\frac{1}{2\sigma_{u/r_0}^2} \left(\frac{u^2}{r_0^2} \right) \right] \quad (u = x \text{ or } y) \quad (6)$$

where $\sigma_{u/r_0} = \sqrt{k_b T_{ion}/2eD}$, n_0 is a coefficient determined by the initial condition of the ions. Hence, from Eq. (6), the pseudopotential depth, D , can be derived from the standard deviation (SD) of ion coordinate σ_u , and the ion temperature T_{ion} . The pseudopotential depth, D , yields

$$D = k_b T_{ion}/2e\sigma_{u/r_0}^2 \quad (7)$$

The ion trapping radius, σ_{u/r_0} (Figure 1b), and ion temperature, $T_{ion} = m\sigma_u^2/k_b$ (Figure 1c), can be numerically obtained from the ion spatial and velocity distributions of the simulated ion cloud, respectively.

The ion trajectory simulations were performed by a home-made electro-hydrodynamic simulation (EHS) package previously developed [27] and validated [28–30]. Five hundred ions with an initial thermal (i.e., Gaussian) distribution, $\sigma_{x/r_0} = 0.04$ and $T_{ion} = 300$ K, were first placed in the trap center; then, they were trapped for more than 10 ms to allow the thermal equilibrium; finally, the properties, σ_{u/r_0} (Figure 1d) and T_{ion} (Figure 1e), of the ion cloud at equilibrium, which was achieved for ion cooling with $t > 6$ ms, was used for calculating the pseudopotential depth, D (light blue region, Figure 1f). For a single ion at 0 Torr, Eq. (7) is equivalent to $D = qV_{RF}/4$ (Supporting Information).

Ion trapping experiments for validation of the simulations were performed in a home-made dual LIT mass spectrometer developed in previous works [31, 32]. The operation parameters of the LITs were as aforementioned unless otherwise

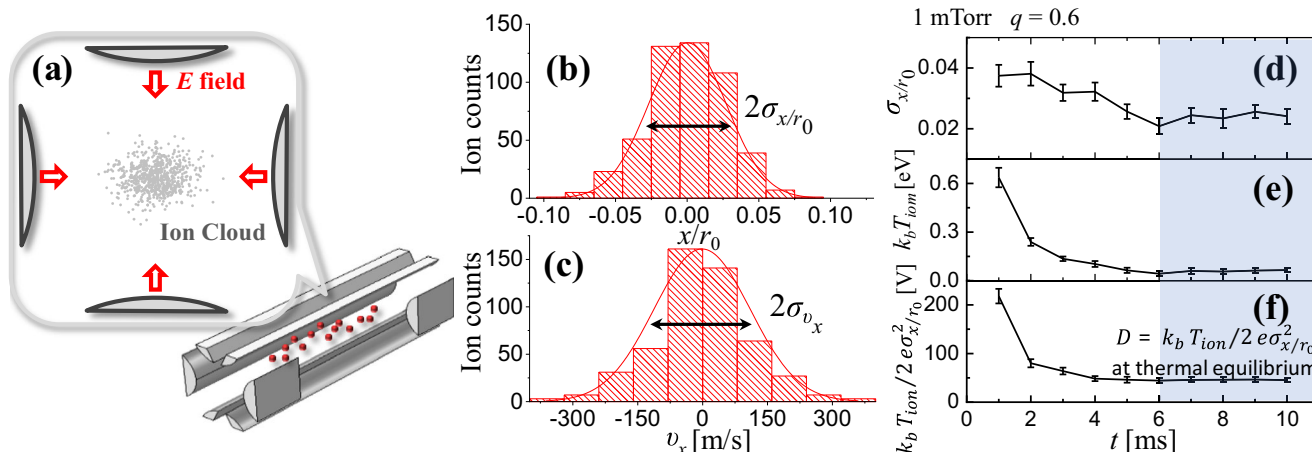


Figure 1. (a) Schematic plot of an ion cloud in the LIT. (b) The spatial and (c) velocity distributions derived from a representative ion cloud. (d) The dimensionless ion trapping radius in the x -direction, σ_x/r_0 ; (e) ion temperature, T_{ion} ; and (f) calculated $k_b T_{ion}/2e\sigma_x^2/r_0$ as a function of time, derived from an ion cloud simulated with $q = 0.6$ at the pressure of 1 mTorr. The error bars represent one standard deviation (SD) for five replicates.

stated. Reserpine ions, m/z 609, were generated by a nano-electrospray ionization (nanoESI) source, operated by a high voltage of 1500 V at atmospheric pressure. The ions were introduced by a discontinuous atmospheric pressure interface of 15 ms to the LIT1 in vacuum for cooling of 500 ms, and then transferred to the LIT2 to measure its ion trapping efficiencies under different background pressures.

Results and Discussion

Eq. (7) shows that the pseudopotential depth, D , of the LIT is proportional to the ion temperature, T_{ion} , and reversely proportional to the square of the ion trapping radius, σ_x , for ion clouds at equilibrium. Ion cloud simulation results showed that the σ_x/r_0 slowly decreased with q first, and then reversed sharply after $q = 0.6\text{--}0.8$ depending on the background pressures (Figure 2a). A more compact ion cloud at equilibrium should have a lower σ_x/r_0 value, and the most compact one was observed at the pressures around 10 mTorr (green curve). Meanwhile, the T_{ion} increased along with q for all the simulated pressures (Figure 2b), due to the increment of the secular frequencies and kinetic energies of the ions, also known as the RF heating effect. At lower q values, $q < 0.4$, the RF heating effect was relatively weak; hence, for pressures above 10 mTorr, the ions were sufficiently cooled by the neutral buffers to the room temperature of 300 K, corresponding to $\frac{1}{2}k_b T_{ion} = 0.013$ eV for x ion motion (indicated by the black arrow, Figure 2b). For higher q values, especially for $q > 0.8$, RF heating dramatically increased, leading to a sharp increment of T_{ion} . Higher pressures were helpful for cooling the ions; the transition point of q , therefore, delayed from $q = 0.6$ at 1 mTorr (red curve) to 0.7 at 10–100 mTorr (green and blue curves) to 0.83 at 2 Torr (cyan curve).

Figure 2c shows the calculated pseudopotential depth, D , of the LIT. It was found that (1) at pressures between 1 and 100

mTorr (red, green, blue curves), the trapping depths, D , were deeper than those at 0 Torr (black curve) and had optimal pressures at around 10 Torr (green curve). For pressures lower than 1 mTorr (red curve), the D would be close to the black curve. For pressures higher than 2 Torr (cyan curve), the D would decrease with pressure. (2) At lower q values, $q < 0.4$, pressures showed little impacts on the trapping depths, D , compared with those at 0 Torr. However, the pressure regulation of D was evident for larger q values, due to the more significant RF heating effect. For instance, at $q = 0.8$, the D at 10 mTorr had a 2-fold improvement compared with that at 0 Torr. Here, it is obvious that the physics of ion trapping with the existence of pressures is strongly related to the flow properties in the vacuum chamber, which cannot be explained by a model based on 0 Torr.

Figure 2d shows the ion trajectories at $q = 0.6$ under different gas flow regimes, characterized by the Knudsen number, $Kn = \lambda/r_0$, where λ is the mean free path of the ions depending on the background pressures. For pressures greater than 100 mTorr in the continuum flow regime ($Kn < 0.1$), the ion trajectory damped continuously with time (blue curve); thus, the decreased trend of D after 100 mTorr could be explained by the decreased effective q , q_{eff} , with the pressure increment [33, 34]. For pressures lower than 1 mTorr in the molecular flow regime ($Kn > 10$), the ion trajectories are almost collision free, like the case of 0 Torr, except for the occasional ion-neutral collisions (black curve). For the pressures in between, the ion trajectory (red curve) was transitional, so as the D . At lower q values, $q < 0.4$, they showed good similarities with the results in the molecular flow (red and black curves in Figure 2c, d); however, the similarity broke at higher q values.

The transitional pressure range of 1 to 100 mTorr is very attractive for ion trap MS [19, 20], which has been widely used for performing mass and tandem MS (MS/MS) analyses. It has long been recognized that this pressure range has better ion trapping efficiencies than the lower pressures, e.g., 10^{-5} Torr.

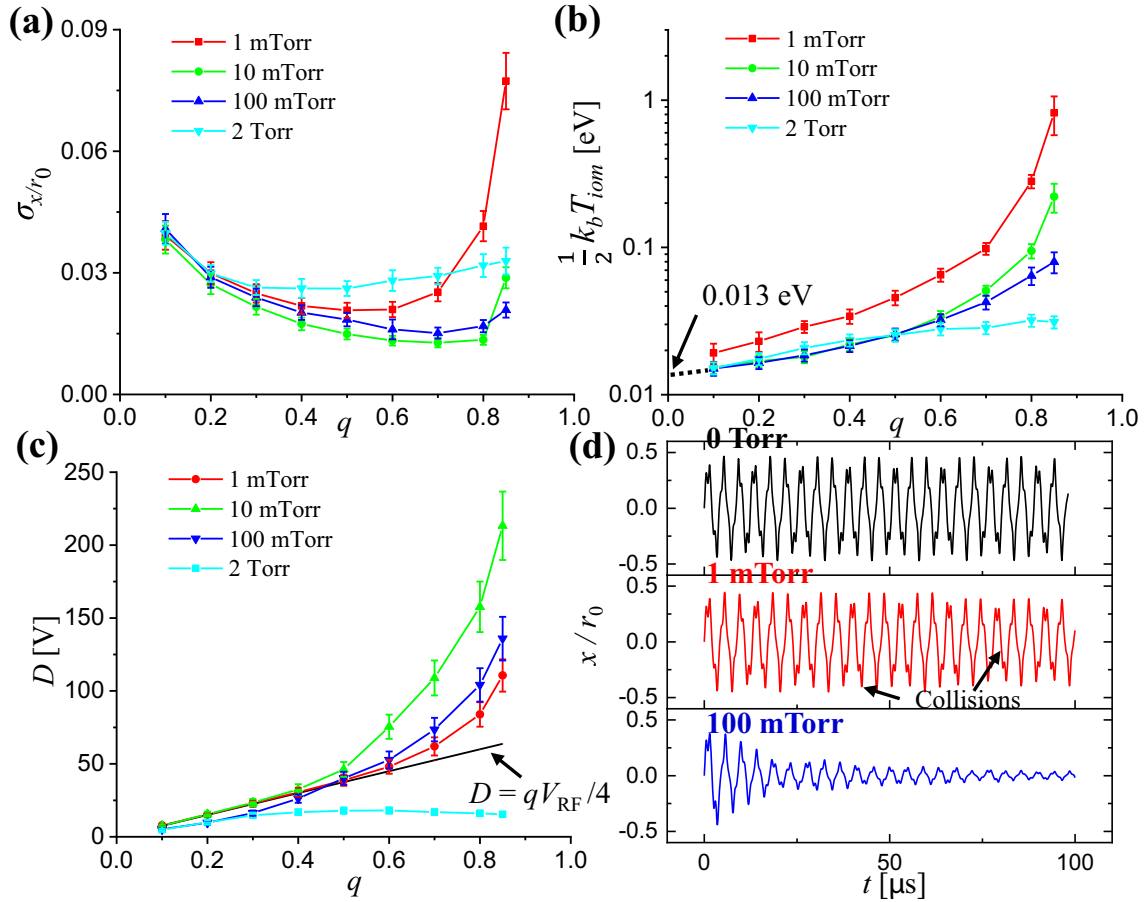


Figure 2. (a) The ion trapping radius σ_{x/r_0} , (b) ion temperature T_{ion} of the ion clouds, and (c) the pseudopotential depth D of the LIT as a function of the Mathieu parameter, q . The ion clouds were thermally equilibrated under different background pressures: 1 mTorr (red curve), 10 mTorr (green curve), 100 mTorr (blue curve), and 2 Torr (cyan curve). The D calculated by using $D = qV_{RF}/4$ considering at a pressure of 0 Torr was shown in black curve. (d) Sing ion trajectories at pressures of 0 Torr (black curve), 1 mTorr (red curve), and 100 mTorr (blue curve) at $q = 0.6$

The ion-neutral collisions might lead to the decrement of effective q , and the decreased trapping depth; therefore, the phenomenon was partially explained by the cooling of the ions, rather than the increment of trapping depths, D [22, 34]. The results of Figure 2c indicated that the improved D , together with the buffer gas cooling effect, is attributable to the improved ion trapping at pressures in the millitorr range. To explore the reason why the D increased in this pressure range, the two factors of D , i.e., σ_{x/r_0} and T_{ion} , were analyzed.

The derivative of D with respect to the pressure, p , according to Eq. (7), yields $\frac{dD}{dp} = \frac{k_b}{2e\sigma_{x/r_0}^2} \left(\frac{dT_{ion}}{dp} - \frac{2k_b T_{ion}}{\sigma_{x/r_0}} \frac{d\sigma_{x/r_0}}{dp} \right)$. Considering that the ion temperature, T_{ion} , monotonically decreased with pressures, i.e., $\frac{dT_{ion}}{dp} < 0$, due to the buffer gas cooling (Figure 3b), the improved D , i.e., $\frac{dD}{dp} > 0$, was attributable to the decreased ion trapping radius $\frac{d\sigma_{x/r_0}}{dp} < 0$ for $p < 10$ mTorr (Figure 3a). For $p > 100$ mTorr, the σ_{x/r_0} became to increase with pressures, $\frac{d\sigma_{x/r_0}}{dp} > 0$ (Figure 3a), giving rise to the drop of D . Note that the σ_{x/r_0} and T_{ion} were more sensitive to pressures at higher q values, e.g., $q = 0.8$ (blue curves), than the lower

ones, e.g., $q = 0.2$ (black curves in Figure 3a, b). This explained the greater D that exceeded the black curve at higher q observed in both the simulation and previous MS experiments [15, 16, 32].

The existence of optimal D in the transitional pressures matched with the ion trapping experiments performed in a dual LIT mass spectrometer (see ‘‘Method’’ for description). Ions in the LIT1 were trapped at $V_{RF} = 600$ V, corresponding to $q = 0.6$ for 300 ms, and then ejected to the LIT2 at the same q with an acceleration voltage of 100 V. Ion trapping efficiencies of the LIT2 under different pressures were measured. It was found that the calculated D could characterize the trend of measured ion intensity in the LIT2 accurately, except that the optimal pressure of 10 mTorr in the simulations shifted to 3 mTorr in the experiments (Figure 3c). The powerful capability of the PW model was the use of D to predict the ion trapping efficiency in the RF systems, as we demonstrated here.

At last, we explored the D and ion trapping near the stability region, where a larger D found in theory, however, led to a poorer ion trapping efficiency that was observed

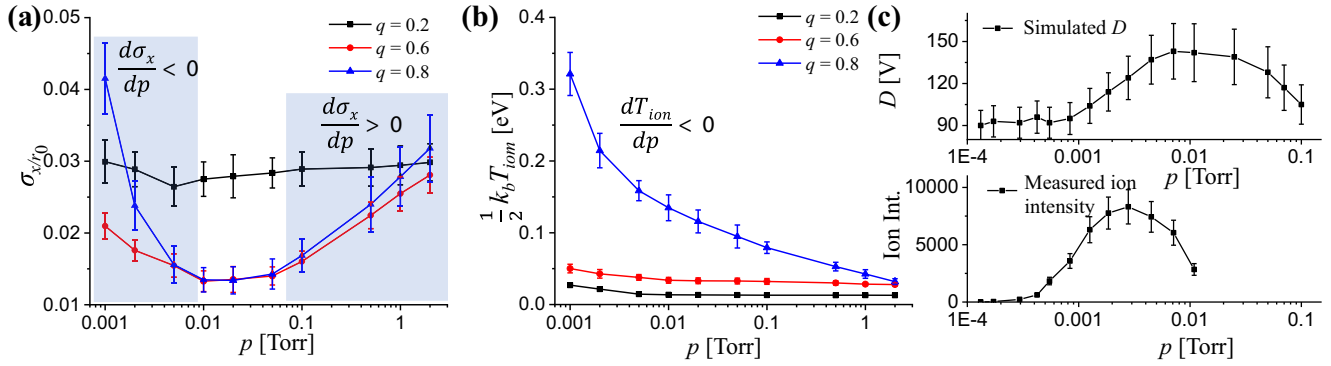


Figure 3. (a) The ion trapping radius σ_x/r_0 and (b) ion temperature T_{ion} as a function of gas pressure for $q=0.2$ (black curve), 0.6 (red curve), 0.8 (blue curve). (c) Simulated D (top panel) and measured ion intensity (bottom panel) as a function of pressure

experimentally [15, 16, 32]. We discussed the difference between the RF and DC trapping and showed that it was the RF heating of the ions that led to the decreased ion trapping efficiencies at higher q values, especially for $q > 0.86$. In the DC trapping, the ions can be ultimately cooled to the room temperature, corresponding to 0.013 eV; however, this is not true for RF trapplings. In the LIT, the ions had a T_{ion} close to room temperature at $q < 0.2$; however, the T_{ion} had a 10-fold increment at around $q = 0.8$ and became comparable with D for $q > 0.86$ (Figure 2b). Note the ion temperature here is due to the RF heating, regardless of the initial ion energies. Hence, the practical trapping depths available, D_a , for ion trapping yields

$$D_a = D - \frac{1}{2}k_b T_{ion} \quad (8)$$

Figure 4 a shows the potential depths, D (black curve) and D_a (red curve), for $q > 0.8$ at 10 mTorr. For $q < 0.85$, the RF heating, $\frac{1}{2}k_b T_{ion}$, was negligibly small. Due to the rapid increment of RF heating to compete with D , a transition of D_a was observed at $q = 0.865$. Note that the D decreased for higher pressures than 10 mTorr; hence, such a transition of D_a at higher pressures would have a shift to lower q values of 0.6–0.8. Other than decreased D_a , significant ion losses were observed for $q > 0.87$ (Figure 4b). For instance, at $q = 0.87$ (red curve) and 0.88 (blue curve), more than 10% and 50% of the ions escaped from the LIT after 10 ms, respectively. The D_a and ion losses shown here matched well with experimental observations previously and explained the poor ion trapping efficiency near the stability boundary.

Conclusion

In conclusion, ion cloud simulation allowed the exploration of the ion-neutral collision effects on the pseudopotential depth, D , of a LIT under a pressure range of 1 mTorr to 2 Torr. Compared with an absolute vacuum, proper pressures of 1 to 100 mTorr were beneficial for the D and ion trapping. An optimal pressure of 10 mTorr was observed to have the most compact ion cloud σ_x/r_0 , and largest, D . The improvement of D

due to pressures was evident for $q > 0.6$; however, the stronger RF heating under ion-neutral collisions at $q > 0.86$ was harmful for ion trapping, leading to the decrement of D_a . In practical ion trap operations, the existence of the nonlinear electric field and

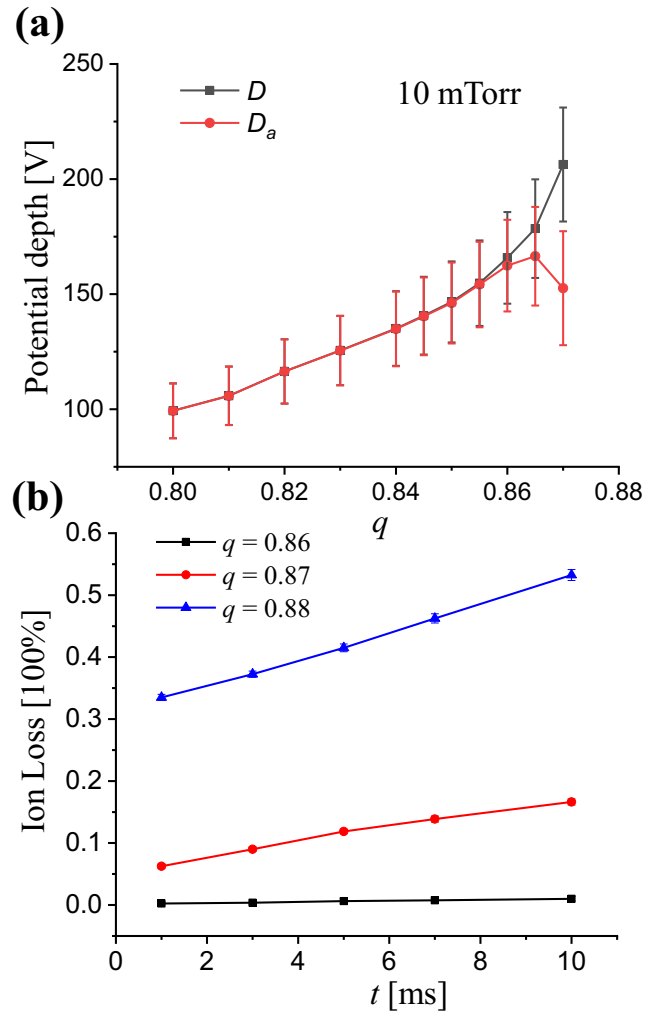


Figure 4. (a) The potential depths, D (black curve) and D_a (red curve), as a function of the Mathieu parameter, q , at 10 mTorr. (b) The ion loss as a function of time for $q = 0.86$ (black curve), 0.87 (red curve), and 0.88 (blue curve)

space charge effect may lead to the shift of q , and the D can be described by $q_{\text{eff}}V_{\text{RF}}/4$, where q_{eff} is the effective q in the nonlinear field. Previously, due to the partial or even incorrect interpretations, the theoretical D mismatched with experimental observations at transitional pressures and near the stability boundary. This study provided valuable evidences to support the correctness of D on describing the RF trapping of ions, demonstrated its universal reliability, and should be helpful for the understanding and improvement of ion trapping in RF devices for ion trap MS.

Acknowledgements

This work was supported by the National Key R&D Program of China (Grant No. 2018YFF0109500) and National Natural Science Foundation of China (Grant Nos. 21705090, 21627807).

References

1. Paul, W., Steinwedel, H.: A new mass spectrometer without a magnetic field. *Z. Naturforsch.* **8A**, 448–450 (1953)
2. Paul, W.: Electromagnetic traps for charged and neutral particles. *Rev. Mod. Phys.* **62**, 531–540 (1990)
3. Maher, S., Jjunju, F.P.M., Taylor, S.: 100 years of mass spectrometry: Perspectives and future trends. *Rev. Mod. Phys.* **87**, 113–135 (2015)
4. Dawson, P.H.: Quadrupole mass analyzers: performance, design and some recent applications. *Mass Spectrom. Rev.* **5**, 1–37 (1986)
5. Peng, Y., Austin, D.E.: New approaches to miniaturizing ion trap mass analyzers. *TrAC Trends Anal. Chem.* **30**, 1560–1567 (2011)
6. Tian, Y., Higgs, J., Li, A., Barney, B., Austin, D.E.: How far can ion trap miniaturization go? Parameter scaling and space-charge limits for very small cylindrical ion traps. *J. Mass Spectrom.* **49**, 233–240 (2014)
7. Kelly, R.T., Tolmachev, A.V., Page, J.S., Tang, K., Smith, R.D.: The ion funnel: theory, implementations, and applications. *Mass Spectrom. Rev.* **29**, 294–312 (2010)
8. Kanu, A.B., Dwivedi, P., Tam, M., Matz, L., Hill Jr., H.H.: Ion mobility–mass spectrometry. *J. Mass Spectrom.* **43**, 1–22 (2008)
9. Dehmelt, H.G.: Radiofrequency spectroscopy of stored ions I: storage. *Adv. At. Mol. Phys.* **3**, 53–72 (1968)
10. Wuerker, R.F., Shelton, H., Langmuir, R.V.: Electrodynamic containment of charged particles. *J. Appl. Phys.* **30**, 342–349 (1959)
11. Douglas, D.J., Berdnikov, A.S., Kononkov, N.V.: The effective potential for ion motion in a radio frequency quadrupole field revisited. *Int. J. Mass Spectrom.* **377**, 345–354 (2015)
12. Gao, C., Douglas, D.J.: Can the effective potential of a linear quadrupole be extended to values of the Mathieu parameter q up to 0.90? *J. Am. Soc. Mass Spectrom.* **24**, 1848–1852 (2013)
13. Sudakov, M.: Effective potential and the ion axial beat motion near the boundary of the first stable region in a nonlinear ion trap. *Int. J. Mass Spectrom.* **206**, 27–43 (2001)
14. Berdnikov, A.S., Douglas, D.J., Kononkov, N.V.: The pseudopotential for quadrupole fields up to $q = 0.9080$. *Int. J. Mass Spectrom.* **421**, 204–223 (2017)
15. Reilly, P.T.A., Brabeck, G.F.: Mapping the pseudopotential well for all values of the Mathieu parameter q in digital and sinusoidal ion traps. *Int. J. Mass Spectrom.* **392**, 86–90 (2015)
16. Xu, W., Li, L., Zhou, X., Ouyang, Z.: Ion sponge: a 3-dimensional array of quadrupole ion traps for trapping and mass-selectively processing ions in gas phase. *Anal. Chem.* **86**, 4102–4109 (2014)
17. Takats, Z., Wiseman, J.M., Gologan, B., Cooks, R.G.: Mass spectrometry sampling under ambient conditions with desorption electrospray ionization. *Science*. **306**, 471–473 (2004)
18. Cooks, R.G., Ouyang, Z., Takats, Z., Wiseman, J.M.: Ambient mass spectrometry. *Science*. **311**, 1566–1570 (2006)
19. Ouyang, Z., Cooks, R.G.: Miniature mass spectrometers. *Annu. Rev. Anal. Chem.* **2**, 187–214 (2009)
20. Snyder, D.T., Pulliam, C.J., Ouyang, Z., Cooks, R.G.: Miniature and fieldable mass spectrometers: recent advances. *Anal. Chem.* **88**, 2–29 (2016)
21. Schwartz, J.C., Senko, M.W., Syka, J.E.P.: A two-dimensional quadrupole ion trap mass spectrometer. *J. Am. Soc. Mass Spectrom.* **13**, 659–669 (2002)
22. Hager, J.W.: A new linear ion trap mass spectrometer. *Rapid Commun. Mass Spectrom.* **16**, 512–526 (2002)
23. Blakeman, K.H., Wolfe, D.W., Cavanaugh, C.A., Ramsey, J.M.: High pressure mass spectrometry: the generation of mass spectra at operating pressures exceeding 1 Torr in a microscale cylindrical ion trap. *Anal. Chem.* **88**, 5378–5384 (2016)
24. Pau, S., Pai, C.S., Low, Y.L., Moxom, J., Reilly, P.T.A., Whitten, W.B., Ramsey, J.M.: Microfabricated quadrupole ion trap for mass spectrometer applications. *Phys. Rev. Lett.* **96**, 120801 (2006)
25. Zhou, X., Ouyang, Z.: Following the ions through a mass spectrometer with atmospheric pressure interface: simulation of complete ion trajectories from ion source to mass analyzer. *Anal. Chem.* **88**, 7033–7040 (2016)
26. Guo, D., Wang, Y., Xiong, X., Zhang, H., Zhang, X., Yuan, T., Fang, X., Xu, W.: Space charge induced nonlinear effects in quadrupole ion traps. *J. Am. Soc. Mass Spectrom.* **25**, 498–508 (2014)
27. Zhou, X., Ouyang, Z.: Flowing gas in mass spectrometer: method for characterization and impact on ion processing. *Analyst*. **139**, 5215–5222 (2014)
28. Zhou, X., Ouyang, Z.: Ion transfer between ion source and mass spectrometer inlet: electro-hydrodynamic simulation and experimental validation. *Rapid Commun. Mass Spectrom.* **30**, 29–33 (2016)
29. Zhou, X., Liu, X., Cao, W., Wang, X., Li, M., Qiao, H., Ouyang, Z.: Study of in-trap ion clouds by ion trajectory simulations. *J. Am. Soc. Mass Spectrom.* **29**, 223–229 (2018)
30. Zhou, X., Liu, X., Chiang, S., Cao, W., Li, M., Ouyang, Z.: Stimulated motion suppression (STMS): a new approach to break the resolution barrier for ion trap mass spectrometry. *J. Am. Soc. Mass Spectrom.* **29**, 1738–1744 (2018)
31. Li, L., Zhou, X., Hager, J.W., Ouyang, Z.: High efficiency tandem mass spectrometry analysis using dual linear ion traps. *Analyst*. **139**, 4779–4784 (2014)
32. Liu, X., Wang, X., Bu, J., Zhou, X., Ouyang, Z.: Tandem analysis by a dual-trap miniature mass spectrometer. *Anal. Chem.* **91**, 1391–1398 (2019)
33. Vinitzky, E.A., Black, E.D., Libbrecht, K.G.: Particle dynamics in damped nonlinear quadrupole ion traps. *Am. J. Phys.* **83**, 313–319 (2015)
34. Whitten, W.B., Reilly, P.T.A., Ramsey, J.M.: High-pressure ion trap mass spectrometry. *Rapid Commun. Mass Spectrom.* **18**, 1749–1752 (2004)